PLASMA IONIZATION BY HELICON WAVES

Francis F. Chen

PPG-1317 July 1990

Electrical Engineering Department and
Institute of Plasma and Fusion Research

To be submitted to *Plasma Physics and Controlled Fusion*

Plasma ionization by helicon waves

Francis F. Chen
Electrical Engineering Department and
Institute for Plasma and Fusion Research
University of California, Los Angeles, CA 90024, U.S.A.

The dispersion relation for helicon waves in a uniform, bounded plasma is derived with both collisional and Landau damping. It is shown that the latter can explain the very high absorption efficiency of helicon waves in plasma sources and can lead to plasma generators with a controlled primary electron energy. The wave pattern and other features of helicon waves are pointed out.

I. INTRODUCTION

Helicon waves were first investigated in the 1960s, first in solid state plasmas (Bowers et al., 1961; Rose et al., 1962; Lehane and Thonemann, 1965), and then in gaseous plasmas (Harding and Thonemann, 1965). The basic theory of these waves was studied extensively in that period (Woods, 1962, 1964; Klozenberg et al., 1965; Davies et al., 1969, 1970). In 1970, Boswell (1970) discovered that a simple, dense plasma source could be made by exciting helicon waves. Interest in such sources was renewed in the 1980s by the emergence of practical applications for them: as gas laser media, as plasma reactors for materials processing, and as plasma lenses for high energy particle beams.

Helicon waves belong to the category of whistler waves, which are right-hand circularly polarized electromagnetic waves in free space. Helicons differ from classical whistlers in two main respects: a) they are of such low frequency that the electrons' gyrations may be disregarded and only their guiding center motions kept, and b) they are modes of bounded systems, in which their purely electromagnetic character cannot be maintained. In a series of experiments, Boswell and co-workers (1982, 1984, 1985, 1987a, 1987b) investigated the structure and propagation of waves in the 7-10 MHz range; showed that peak densities of order 10^{13} cm^{-3} (in argon), fully ionized on axis, could be created in 10-cm diameter tubes with only 1 kW of rf power and 1 kG of magnetic field; and studied the effects of varying the tube diameter, antenna configuration, and input gas. Using a helicon generator with 1 kW at the industrial frequency of 13.56 MHz, Perry and Boswell (1989) have measured the etch rate of Si and SiO_2 in an SF_6 plasma. With higher powers (3.5kW, 7MHz, 750G), it has been possible to produce densities approaching 10^{14} cm^{-3} in an argon laser application (Zhu and Boswell, 1989).

In Boswell's experiments, however, the calculated collisional absorption rate for helicon waves was much too low to explain the efficient ionization observed. Moreover, the measured wave profiles were consistent with theory only if the collision rate had been 1000 times the classical one. In 1985, Chen (1985) pointed out that Landau damping could be the cause of the efficient energy absorption. This mechanism, if it is operative, could be used even more effectively by directly accelerating the primary electrons (Chen, 1987). Experiments set up to prove this hypothesis have indeed given indications of Landau damping (Chen, 1989) and of electron acceleration (Chen and Decker, 1989, 1990).

The remarkable efficiency of helicon sources can be illustrated by the following simple calculation of density in a non-fusion plasma without axial confinement. Consider a cylinder with a magnetic field strong enough to confine electrons radially but too weak to confine the ions. An ambipolar potential then builds up to confine the ions radially. In the axial direction, sheaths on the endplates arise to confine the electrons, but the ions are not confined

and can escape at the acoustic velocity c_s. The loss rate dN/dt is then $2\pi a^2 n c_s$, a being the radius. Let W be the average power needed to produce each ion-electron pair. W is usually of order 200 eV, since the primary electrons lose many times as much energy in inelastic collisions as they do in ionizing collisions. The power required to maintain the discharge is then $P = WdN/dt = 2\pi a^2 n c_s W$. Taking $a = 5$cm and $c_s = 2.8 \times 10^5$ cm/sec ($T_e = 3eV$, argon), we obtain

$$n(\mathrm{cm}^{-3}) = 7 \times 10^{11} P(kW) \quad .$$

A peak density of $10^{13}\mathrm{cm}^{-3}$ with 1 kW of rf power, or an average density of $\sim 5 \times 10^{12}$ cm^{-3}, is an order of magnitude improvement over that in ordinary discharges and brings W down to the order of the ionization energy. We hypothesize that this is possible if the ionizing electrons are directly accelerated by the wave-particle interaction rather than by a random heating process. This paper gives the theoretical basis for this hypothesis.

II. DISPERSION RELATION

Helicon waves in their simplest form are derived from these three linearized equations (in SI units):

$$\nabla \times \mathbf{E} = -\partial \mathbf{B}/\partial t \tag{1}$$

$$\nabla \times \mathbf{B} = \mu_o \mathbf{j} \tag{2}$$

$$\mathbf{E} = \mathbf{j} \times \mathbf{B}_o / e n_o \quad , \tag{3}$$

where n_o and $\mathbf{B}_o = B_o \hat{z}$ are the equilibrium density and magnetic field, and n, $\mathbf{B}$, $\mathbf{E}$, and $\mathbf{j}$ the perturbed density, magnetic and electric fields, and current, respectively. Eqs. (1-3) further imply

$$\nabla \cdot \mathbf{B} = 0 \tag{4}$$

$$\nabla \cdot \mathbf{j} = 0 \tag{5}$$

$$\mathbf{j}_\perp = -e n_o \mathbf{E} \times \mathbf{B}_o / B_o^2 \quad . \tag{6}$$

In Eq. (2) we have neglected the displacement current. In Eq. (3), we have assumed that the plasma current is entirely carried by the $\mathbf{E} \times \mathbf{B}$ guiding center drift of the electrons; that is, that (a) $\omega \ll \omega_c$ so that the electrons' cyclotron motion is too fast to matter, (b) ω is much higher than the lower hybrid frequency so that ion motions can be neglected, and (c)

the resistivity is zero, so that $E_z = 0$. Dissipation effects will be added in the next section. Without these effects, an arbitrary current j_z can be supported, while the perpendicular component of $\mathbf{j}$ is given in Eq. (6).

We assume perturbations of the form $\exp i(m\theta + kz - \omega t)$, representing wave patterns that rotate in the clockwise ($m > 0$) or counterclockwise ($m < 0$) direction in time at a given position z when viewed in the $\mathbf{B}_o$ direction. Eqs. (1) and (3) give

$$\begin{aligned} i\omega\mathbf{B} &= \nabla \times \mathbf{E} = \nabla \times (\mathbf{j} \times \mathbf{B}_o)/en_o \\ &= (\mathbf{B}_o \cdot \nabla)\mathbf{j}/en_o = (ikB_o/en_o)\mathbf{j} \ , \end{aligned} \tag{7}$$

and using Eq. (2) for $\mathbf{j}$ yields

$$\mathbf{B} = \left(\frac{\omega}{k}\frac{\mu_o e n_o}{B_o}\right)^{-1} \nabla \times \mathbf{B} \ . \tag{8}$$

We define the quantity α, which can be expressed in terms of the usual electron frequencies ω_p and ω_c:

$$\alpha \equiv \frac{\omega}{k}\frac{\mu_o e n_o}{B_o} = \frac{\omega}{k}\frac{\omega_p^2}{\omega_c c^2} \ . \tag{9}$$

Eq. (8) then becomes

$$\nabla \times \mathbf{B} = \alpha \mathbf{B} \ , \tag{10}$$

whose curl gives our main equation

$$\nabla^2 \mathbf{B} + \alpha^2 \mathbf{B} = 0 \ . \tag{11}$$

Substituting Eq. (10) into Eq. (2) gives

$$\mathbf{j} = (\alpha/\mu_o)\mathbf{B} \ , \tag{12}$$

showing that the current is parallel to the wave magnetic field; all three components of both are important.

Denoting $\partial/\partial r$ by ($'$), we may write the z component of Eq. (11) in cylindrical coordinates as follows:

$$B_z'' + \frac{1}{r}B_z' + \left(T^2 - \frac{m^2}{r^2}\right) B_z = 0 \ , \tag{13}$$

where the transverse wavenumber T is defined as

$$T^2 \equiv \alpha^2 - k^2 \quad . \tag{14}$$

This is Bessel's equation, and the solution which is finite at $r = 0$ is $J_m(Tr)$:

$$B_z = C_3 J_m(Tr) \quad . \tag{15}$$

The r and θ components of Eq. (10) are

$$\frac{im}{r} B_z - ikB_\theta = \alpha B_r \tag{16}$$

$$ikB_r - B_z' = \alpha B_\theta \quad . \tag{17}$$

Solving for B_r and B_θ in terms of B_z and B_z', and substituting for B_z from Eq. (15), we obtain

$$B_r = \frac{iC_3}{T^2}\left(\frac{m}{r}\alpha J_m + kJ_m'\right) \tag{18}$$

$$B_\theta = -\frac{C_3}{T^2}\left(\frac{m}{r}kJ_m + \alpha J_m'\right) \quad . \tag{19}$$

Use of the recursion relations

$$\frac{m}{r}J_m = \frac{T}{2}(J_{m-1} + J_{m+1}) \,, \qquad J_m' = \frac{T}{2}(J_{m-1} - J_{m+1}) \tag{20}$$

yields

$$B_r = \frac{iC_3}{2T}[(\alpha + k)J_{m-1} + (\alpha - k)J_{m+1}] \tag{21}$$

$$B_\theta = -\frac{C_3}{2T}[(\alpha + k)J_{m-1} - (\alpha - k)J_{m+1}] \quad . \tag{22}$$

Introducing the amplitude

$$A \equiv iC_3/2T \quad , \tag{23}$$

we may write Eqs. (21), (22) and (15) as

$$B_r = C_1 J_{m-1} + C_2 J_{m+1} \tag{24}$$

$$B_\theta = i(C_1 J_{m-1} - C_2 J_{m+1}) \tag{25}$$

$$B_z = C_3 J_m \quad , \tag{26}$$

where

$$C_1 = (\alpha + k)A, \qquad C_2 = (\alpha - k)A, \qquad C_3 = -2iTA \quad . \tag{27}$$

For future reference we give here the right- and left-hand circular components B_R, B_L of the local field as defined by

$$\sqrt{2}B_R \equiv B_r - iB_\theta \quad , \qquad \sqrt{2}B_L \equiv B_r + iB_\theta \tag{28}$$

and the inverse transformation

$$\sqrt{2}B_r = B_R + B_L \quad , \qquad \sqrt{2}B_\theta = i(B_R - B_L) \quad : \tag{29}$$

$$B_R = \sqrt{2}C_1 J_{m-1}(Tr) \quad , \quad B_L = \sqrt{2}C_2 J_{m+1}(Tr) \quad , \quad B_z = C_3 J_m(Tr) \quad . \tag{30}$$

The electric field $\mathbf{E}$ is given by Eq. (1):

$$E_r = (\omega/k)B_\theta, \qquad E_\theta = -(\omega/k)B_r, \qquad E_z = 0 \quad , \tag{31}$$

or, equivalently,

$$E_R = i(\omega/k)B_R \quad , \qquad E_L = -i(\omega/k)B_L \quad , \qquad E_z = 0 \quad . \tag{32}$$

The transverse components are thus

$$E_r \;=\; i(\omega/k)(C_1 J_{m-1} - C_2 J_{m+1}) \tag{33}$$

$$E_\theta \;=\; -(\omega/k)(C_1 J_{m-1} + C_2 J_{m+1}) \quad , \tag{34}$$

with C_1 and C_2 given by Eq. (27).

The boundary condition for an insulator is $j_r = 0$ at $r = a$; that is, from Eq. (12), $B_r = 0$. A conducting boundary would require $E_\theta = 0$, or, from Eq. (31), $B_r = 0$. Thus, for this case of the simplest helicon, it does not matter whether the tube is insulating or conducting. Eq. (18) then gives the boundary condition

$$m\alpha J_m(Ta) + ka\, J'_m(Ta) = 0 \quad , \tag{35}$$

where $J'_m(Ta)$ is the r-derivative of $J_m(Tr)$ at $r = a$. In particular, the lowest two azimuthal modes are given by

$$J_1(Ta) = 0 \qquad (m = 0) \tag{36}$$

$$J_1(Ta) = (ka\,T/2\alpha)\,(J_2 - J_o) \simeq 0 \qquad (m = 1) \tag{37}$$

The last inequality holds for long, thin tubes, where $T \simeq \alpha$ and $ka \ll 1$. To obtain the dispersion relation $\omega(k)$ for given n_o, B_o, and a, one can proceed as follows. Defining $Z \equiv Ta$ and $\kappa \equiv ka$, one can substitute for α from Eq. (14) and write Eq. (37) for the $m = 1$ mode, for instance, as follows:

$$J_1(Z) = -\frac{\kappa Z}{\alpha a} J_1'(Z) = \frac{\kappa Z}{2\alpha a}[J_2(Z) - J_o(Z)] \quad , \tag{38}$$

where $J'(Z) = dJ(Z)/dZ$ and $\alpha a = (Z^2 + \kappa^2)^{\frac{1}{2}}$. This can be solved by iteration for $Z(\kappa)$. In most cases, however, Z will be such a weak function of κ that we can obtain a good approximation for any $m > 0$ by using the Taylor expansion of $J_m(Z_m)$ about Z_m, where Z_m is the root of $J_m(Z_m) = 0$. Thus

$$J_m(Z) \simeq J_m(Z_m) + (Z - Z_m)J_m'(Z_m) = (Z - Z_m)J_m'(Z_m) \quad . \tag{39}$$

From Eq. (35), we have

$$J_m(Z) = -(\kappa/m\alpha a)J_m'(Z) \simeq -(\kappa/m\alpha_m a)J_m'(Z_m) \quad , \tag{40}$$

where $\alpha_m^2 a^2 \equiv Z_m^2 + \kappa^2$. Eqs. (39) and (40) give $Z \simeq Z_m - \kappa/m\alpha_m a$. Using this in the definition $\alpha a = (Z^2 + \kappa^2)^{\frac{1}{2}}$ and expanding to lowest order in $\kappa/Z = k/T$, we obtain a value of α which can be used in Eq. (9). The resulting approximate dispersion relation for $m > 1$ can then be written

$$\frac{B_o}{n_o} = \frac{e\mu_o a}{Z_m}\left(\frac{\omega}{k} + \frac{\omega}{mZ_m^2}\right) \quad , \tag{41}$$

where $Z_m = 3.83$ for $m = 1$. The second term is a small correction of order k/T and is essentially an additive constant. We see that B/n is proportional to the phase velocity; that is, to the square root of the accelerated electron energy E_f. Thus, if E_f has an optimum value for efficient ionization, the ratio n/B tends to be constant.

III. STRUCTURE OF HELICON MODES

The wave fields are given by Eqs. (24-26), (27), and (31). Including the real part of the exponential factor, these can be written

$$B_r = -\frac{k}{\omega}E_\theta = A\,[(\alpha + k)J_{m-1}(Tr) + (\alpha - k)J_{m+1}(Tr)]\cos(m\theta + kz - \omega t) \tag{42}$$

$$B_\theta = \frac{k}{\omega}E_r = -A\,[(\alpha + k)J_{m-1}(Tr) - (\alpha - k)J_{m+1}(Tr)]\sin(m\theta + kz - \omega t) \tag{43}$$

$$B_z = 2ATJ_m(Tr)\sin(m\theta + kz - \omega t) \ , \qquad E_z = 0. \tag{44}$$

With the recursion relations Eq. (20), Eqs. (42) and (43) can be written alternatively as

$$B_r = -\frac{k}{\omega}E_\theta = \frac{2A}{T}\left[\frac{m\alpha}{r}J_m(Tr) + kJ'_m(Tr)\right]\cos(m\theta + kz - \omega t) \tag{45}$$

$$B_\theta = \frac{k}{\omega}E_r = -\frac{2A}{T}\left[\alpha J'_m(Tr) + \frac{mk}{r}J_m(Tr)\right]\sin(m\theta + kz - \omega t) \ . \tag{46}$$

We note that the **E** and **B** fields are orthogonal to each other on each constant-z plane. In addition, **B** has a z-component to preserve its divergenceless nature, but **E** does not. Indeed, **E** has a finite divergence, proportional to a large space charge which would not arise in free space and which greatly affects the wave pattern. From Eqs. (3), (12), (9), and (10), the divergence of **E** is found to be

$$\begin{aligned} \nabla\cdot\mathbf{E} &= \nabla\cdot(\mathbf{j}\times\mathbf{B}_o)/en_o = \mathbf{B}_o\cdot(\nabla\times\mathbf{j}) \\ &= \frac{B_o}{en_o}\left[\nabla\times\frac{\alpha}{\mu_o}\mathbf{B}\right]_z = \frac{\omega}{k}\left[\nabla\times\mathbf{B}\right]_z = \frac{\omega}{k}\alpha B_z. \end{aligned} \tag{47}$$

Thus, the space charge is proportional to B_z and is peaked on axis for the $m = 0$ mode and at the peak of J_1 ($Tr = 1.84$) for the $m = 1$ mode. We now examine the $m = 0$ and $m = \pm 1$ modes in more detail.

The $m = 0$ mode. For the $m = 0$ mode, we have, from Eq. (20), $J_{-1} = -J_1$ and $J'_o = -TJ_1$. Eqs. (44-46) can then be written

$$B_r = -AkJ_1(Tr)\cos\psi\,, \qquad E_r = A\omega(\alpha/k)J_1(Tr)\sin\psi \tag{48}$$

$$B_\theta = A\alpha J_1(Tr)\sin\psi\,, \qquad E_\theta = A\omega J_1(Tr)\cos\psi \tag{49}$$

$$B_z = ATJ_o(Tr)\sin\psi\,, \qquad E_z = 0\,, \tag{50}$$

where $\psi = kz - \omega t$. The boundary condition $J_1(Ta) = 0$ gives $Ta = 3.83$ for the lowest radial mode regardless of the value of k/α. It is seen that B_z peaks on axis and that B_r and B_θ both peak at $r/a = 1.84/3.83 = 0.48$, the ratio B_r/B_θ being independent of radius. Furthermore, Eqs. (30) and (27) show that $|B_R/B_L| = (\alpha+k)/(\alpha-k)$, so that, for $|k/\alpha| < 1$, the local fields are elliptically polarized in the right-hand direction for $k > 0$ and in the left-hand direction for $k < 0$. Eqs. (48) and (49) show that the long axis of the ellipse is in the r direction for **E** and in the θ direction for **B**.

The electric field pattern is shown in Fig. 1. When $\psi = 0$, E_r vanishes, and the field is purely electromagnetic. When $\psi = \pi/2$, the field is purely radial and electrostatic. In

between, the field lines are spiral. Since $|\alpha/k|$ is normally $\gg 1$, the radial, electrostatic component of $\mathbf{E}$ dominates over the azimuthal, electromganetic component, suggesting that coupling to this mode is best done through the electrostatic field. The smaller $|k/\alpha|$ is, the smaller the range of phase angles ψ over which the electromagnetic component of $\mathbf{E}$ can be seen; and in the limit $k/\alpha = 0$, the E-field is always radial (a space charge field), changing sign at $\psi = \pi/2$.

The $m = \pm 1$ modes. By contrast, the $m = +1$ mode has a field pattern that does not change with position; but it does change with the value of $|k/\alpha|$. The electric field pattern is given by

$$E_r = -\frac{A}{T}\frac{\omega}{k}\left[\alpha J_1'(Tr) + \frac{k}{r}J_1(Tr)\right]\sin(\theta + kz - \omega t) = \frac{\omega}{k}B_\theta \tag{51}$$

$$E_\theta = -\frac{A}{T}\frac{\omega}{k}\left[\frac{\alpha}{r}J_1(Tr) + kJ_1'(Tr)\right]\cos(\theta + kz - \omega t) = -\frac{\omega}{k}B_r \ , \tag{52}$$

with $E_z = 0$. This pattern simply rotates as z changes so as to keep $\theta + kz$ constant, as shown in Fig. 2a. By using the recursion relations Eq. (20), we can describe the E-field at $kx - \omega t = 0$ as follows:

$$E_r = E_o(\beta J_o - J_2)\sin\theta \tag{53}$$

$$E_\theta = E_o(\beta J_o + J_2)\cos\theta \ , \tag{54}$$

where

$$\beta \equiv [1 + (k/\alpha)]/[1 - (k/\alpha)] \ , \tag{55}$$

and the Bessel functions have argument Tr. The E-field lines are shown in Fig. 2b for $k/\alpha = 1/3$. Since $\mathbf{E}$ must be perpendicular to the boundary, it is clear that $\mathbf{E}$ is plane polarized at $r = a$. Near the axis, the $m = 1$ mode is right-hand polarized, since, from Eqs. (30) and (32), $B_R \propto J_o$ and $B_L \propto J_2$, so that $|B_R| \gg |B_L|$. In between, there is a region in which $|J_2(Tr)| > |J_o(Tr)|$ so that $\mathbf{E}$ is left-hand elliptically polarized. These conditions are obviously satisfied by rotation of the pattern shown in Fig. 2b.

The lines of $\mathbf{E}$ in Fig. 2 are not closed because of the space charge [Eq. (47)]. An $m = 1$ antenna can be designed to couple to the strong, straight electrostatic field near the center. The lines of $\mathbf{B}_\perp$ are orthogonal to $\mathbf{E}$ and also have a divergence. In this case, there is a component B_z given by Eq. (30) which closes the B-lines to preserve $\nabla \cdot \mathbf{B} = 0$. The transverse components of $\mathbf{B}$ induce an electromagnetic E_z which cancels the E_z caused by the space charge; in this way, the total E_z is made zero, as it has to be in the absence of damping.

For each value of k/α, the value of T is given by the solution of Eq. (54):

$$\beta J_o(Ta) + J_2(Ta) = 0 \quad . \tag{56}$$

The field pattern of Fig. 2b shows a separatrix that separates lines that reach the boundary from those that are confined. All the field lines converge on a point at a radius r_o. Since E_r must vanish there, r_o is given by the solution of Eq. (53):

$$\beta J_o(Tr_o) - J_2(Tr_o) = 0 \quad . \tag{57}$$

It will be shown in the next section that the absorption of wave energy varies as $J_m(Tr)$, so that the radius of maximum energy deposition is given by $J_1'(Tr_m) = 0$. As k/α varies, the quantities T, r_o/a, and r_m/a vary in the manner shown in Fig. 3. The field pattern remains similar to that of Fig. 2b; only r_o changes. The separation betwen r_o and r_m increases with k/α. In the limit $k/\alpha = 0$, r_o merges with r_m, and the pattern becomes the same as that of the TM_{11} electromagnetic mode in a vacuum waveguide.

Similarly, the $m = -1$ mode has left-hand circular polarization near the axis, changing to right-hand elliptical polarization and then to plane polarization near the boundary. By summing $m = +1$ and $m = -1$ modes, one can attempt to construct a mode that is nearly plane-polarized everywhere, and thus susceptible to being driven by a non-helical antenna. Discussion of this interesting problem will be given in a separate paper.

The relation between the wave pattern shown in Fig. 2b and that of pure electromagnetic waves in a circular waveguide can be seen as follows. When there is no plasma, the only current is the displacement current, and Eq. (2) is replaced by

$$\nabla \times \mathbf{B} = -i\omega\epsilon_o\mu_o\mathbf{E} \quad . \tag{58}$$

The wave equation (11) then becomes

$$\nabla^2\mathbf{B} + k_o^2\mathbf{B} = 0 \quad , \tag{59}$$

where $k_o^2 \equiv \omega^2/c^2$. This is identical with Eq. (11), so the solutions of Eqs. (24-26) and (31) are still valid if we define T in Eq. (14) with k_o in place of α. However, the coefficients C_j are different. The condition $\nabla \cdot \mathbf{B} = 0$ gives

$$iC_3 = T(C_1 - C_2)/k \tag{60}$$

in agreement with Eq. (27), but now we have $\nabla \cdot \mathbf{E} = 0$ also. This yields

$$\nabla \cdot \mathbf{E} = -i(\omega/k)(C_1 + C_2)TJ_m = 0 \quad , \tag{61}$$

showing that $C_1 = -C_2$. For the helicon wave when $\alpha \gg k$, we see from Eq. (27) that $C_1 \simeq C_2$. This reversal of sign means that the roles of B_r and B_θ are interchanged, as is easily seen from Eqs. (24) and (25). The field lines are therefore almost orthogonal to one another in the helicon and vacuum cases, and the lines of $\mathbf{E}$ and of $\mathbf{B}$ are roughly interchanged. Indeed, the TE helicon mode resembles the TM electromagnetic mode. This shows the importance of the space charge field in helicon waves.

IV. COLLISIONAL AND COLLISIONLESS DAMPING

Damping of helicon waves arises, as with Alfvén waves, from the drag on electron motion along $\mathbf{B}$ caused by collisions or by Landau damping. A component E_z is then needed to push the electrons in that direction. To arrive at simple formulas for the damping, we assume the ordering $\nu \ll \omega \ll \omega_c$, which is valid over a wide parameter regime. For instance, with $n_o = 6 \times 10^{12}\text{cm}^{-3}$, $B_o = 100G$, $T_e = 3eV$, and $f = 27$ MHz, we have $\nu_{ei} = 1.7 \times 10^7$, $\omega = 1.7 \times 10^8$, and $\omega_c = 1.76 \times 10^9\,\text{sec}^{-1}$, so that the frequencies are separated by about an order of magnitude. The electron collision rate with neutrals is negligible compared with the rate ν_{ei} with ions for all but the weakest discharges. Electron inertia is then negligible in the perpendicular motion, but it is dominant in the motion parallel to the magnetic field. Therefore, to account for collisional drag and parallel inertia, we need to change only the equation for j_z, leaving the perpendicular equations unaltered. For fields much below 100G, the electrons' gyratory motion and perpendicular inertia have to be considered, as has been pointed out by Davies (1970); we shall treat this case in a separate paper. Kinetic effects in the perpendicular direction have to do with finite electron Larmor radius and also may be neglected except at the lowest magnetic fields.

A. Collisional damping

The linearized equation of motion for a cold electron fluid with a phenomenological collision rate ν yields the following replacement for Eq. (3):

$$\mathbf{E} = \frac{\mathbf{j} \times \mathbf{B}_o}{en_o} - \frac{im}{n_o e^2}(\omega + i\nu)\mathbf{j} \quad . \tag{62}$$

Eqs. (1), (2), and (62) are now the governing equations. Substituting for $\mathbf{j}$ from Eq. (2), taking the curl of Eq. (62), and combining with Eq. (1), we obtain

$$(\omega + i\nu)\nabla \times \nabla \times \mathbf{B} - k\omega_c \nabla \times \mathbf{B} + \alpha k \omega_c \mathbf{B} = 0 \quad . \tag{63}$$

This can be factored as

$$(\beta_1 - \nabla\times)(\beta_2 - \nabla\times)\mathbf{B} = 0 \ , \tag{64}$$

where β_1 and β_2 are the roots of the quadratic

$$(\omega + i\nu)\beta^2 - k\omega_c\beta + k\omega_c\alpha = 0 \ . \tag{65}$$

The most general solution of Eq. (64) is $\mathbf{B} = \mathbf{B}_1 + \mathbf{B}_2$, where

$$\nabla \times \mathbf{B}_1 = \beta_1\mathbf{B}_1, \qquad \nabla \times \mathbf{B}_2 = \beta_2\mathbf{B}_2; \ . \tag{66}$$

The solutions of Eq. (65) are

$$\beta_{1,2} = [1 \mp (1 - 4\alpha\gamma)^{\frac{1}{2}}]/2\gamma \ , \tag{67}$$

where

$$\gamma \equiv (\omega + i\nu)/k\omega_c \ , \tag{68}$$

and α is defined in Eq. (9). The root β_1 is the one corresponding to the helicon wave, since $\beta_2 \simeq 1/2\gamma$ is not close to α. For small $\alpha\gamma$, β_1 is approximately

$$\beta_1 = \frac{1}{2\gamma}[1 - (1 - 4\alpha\gamma)^{\frac{1}{2}}] \cong \alpha(1 + \alpha\gamma) \ . \tag{69}$$

Writing γ in terms of α according to Eq. (9), we obtain

$$\beta_1 = \alpha\left[1 + \left(\frac{\alpha c}{\omega_p}\right)^2\left(1 + \frac{i\nu}{\omega}\right)\right] \ . \tag{70}$$

When ν is the electron-ion collision frequency ν_{ei}, the plasma resistivity η is given by

$$\eta = m\nu/n_o e^2 \ , \tag{71}$$

and β_1 can also be written

$$\beta_1 = \alpha\left[1 + \alpha^2\left(\frac{c^2}{\omega_p^2} + \frac{i\eta}{\mu_o\omega}\right)\right] \ . \tag{72}$$

Since Eq. (66) is identical with Eq. (10), the previous solutions are unchanged except for the substitution of β_1 for α in Eqs. (10) and (14):

$$T^2 = \beta_1^2 - k^2 \ . \tag{73}$$

To satisfy the boundary conditions, T must be real; hence, k must be complex when β_1 is complex. To find $Im(k)$, we define

$$k = k_r + k_i \ , \qquad \delta \equiv k_i/k_r \ . \tag{74}$$

Since α varies as $1/k$, we can write it as

$$\alpha = \alpha_o(1 + i\delta)^{-1} \ , \qquad \alpha_o \equiv \frac{\omega}{k_r}\frac{\omega_p^2}{\omega_c c^2} \ . \tag{75}$$

The complex value of k can then be found by substituting Eq. (75) into Eq. (70) and Eq. (70) into Eq. (73), and then setting the imaginary part of Eq. (73) to zero. When the damping is small, we can expand Eq. (70) for small δ and ν/ω. To first order in these quantities, Eq. (73) yields

$$\frac{k_i}{k_r} = \frac{\nu}{\omega}\left(\frac{\alpha_o c}{\omega_p}\right)^2 \Big/ \left(1 + \frac{k_r^2}{\alpha_o^2}\right) \simeq \frac{\nu}{\omega}\left(\frac{\alpha_o c}{\omega_p}\right)^2 \ . \tag{76}$$

The last inequality holds for $T \gg k$. The damping rate is then approximately

$$Im(k) \simeq \alpha\nu/\omega_c \simeq (\nu/\omega_c)T \ , \tag{77}$$

or, in terms of resistivity,

$$\frac{Im(k)}{Re(k)} \simeq \frac{\alpha_o^2}{\omega}\frac{\eta}{\mu_o} \ . \tag{78}$$

The collisional damping length $L_c = 1/Im(k)$ can be written

$$L_c \simeq \frac{\omega_c}{\nu T} \simeq \frac{\omega}{k}\frac{\mu_o}{\eta T^2} \ . \tag{79}$$

B. Landau damping

In the absence of collisions, the electron motion along $\mathbf{B}_o$ is controlled by electron inertia and wave-particle interactions. The inertia effect was included in the previous section in the limit $\nu = 0$, but the Landau effect has to be treated kinetically. On the other hand, the kinetic effect in the transverse direction involves the finite Larmor radius of the electrons and can be neglected at all but the lowest magnetic fields. For $\omega \ll \omega_c$, the inertia effect in the transverse direction can also be neglected, the plasma behaving like a hydromagnetic fluid in that direction. Our previous treatment, therefore, needs to be changed only in the use of the Boltzmann equation to solve for the electron parallel velocities.

To make an eventual connection with the collisional results, we write the Boltzmann-Vlasov equation with a particle-preserving Krook collision term:

$$\frac{\partial f_1}{\partial t} + v\frac{\partial f_1}{\partial z} - \frac{e}{m}E\frac{\partial f_o}{\partial v} = \left(\frac{n_1}{n_o}f_o - f_1\right)\nu \quad . \tag{80}$$

Here the subscript z on E and v has been suppressed, and the equation has been linearized. For f_1 varying as $\exp i(kz - \omega t)$, the solution is

$$f_1(v) = \frac{ieE}{m}\frac{f_o'(v)}{\omega + i\nu - kv} + i\nu\frac{n_1}{n_o}\frac{f_o(v)}{\omega + i\nu - kv} \quad . \tag{81}$$

Since the last term already contains ν, we may approximate n_1 with the solution of the collisionless Vlasov equation:

$$n_1 = \int_{-\infty}^{\infty} f_1(v)dv \ , \tag{82}$$

$$f_1(v) = \frac{ieE}{m}\frac{f_o'(v)}{\omega - kv} \quad . \tag{83}$$

With the definitions

$$u \equiv v/v_{\rm th} \ , \qquad v_{\rm th}^2 \equiv 2KT_e/m \tag{84}$$

$$\zeta_o \equiv \omega/kv_{\rm th} \ , \qquad \zeta \equiv (\omega + i\nu)/kv_{\rm th} \ , \tag{85}$$

this becomes

$$n_1 = \frac{ieE}{mkv_{\rm th}}\int_{-\infty}^{\infty}\frac{f_o'(u)du}{\zeta_o - u} \quad . \tag{86}$$

Specifying a Maxwellian distribution

$$f_o(u) = \frac{n_o}{\sqrt{\pi}v_{\rm th}}e^{-u^2} \tag{87}$$

and integrating by parts, we have for n_1

$$n_1 = -\frac{ien_oE}{mkv_{\rm th}^2}\frac{1}{\sqrt{\pi}}\int_{-\infty}^{\infty}\frac{e^{-u^2}du}{(u-\zeta_o)^2} \quad . \tag{88}$$

In terms of the plasma dispersion function defined by

$$Z(\zeta) \equiv \frac{1}{\sqrt{\pi}}\int_{-\infty}^{\infty}\frac{e^{-u^2}du}{u-\zeta} \ , \qquad Z'(\zeta) = \frac{1}{\sqrt{\pi}}\int_{-\infty}^{\infty}\frac{e^{-u^2}du}{(u-\zeta)^2} \ , \tag{89}$$

we finally obtain

$$\frac{n_1}{n_o} = -\frac{ieE}{mkv_{th}^2} Z'(\zeta_o) \quad . \tag{90}$$

With this value of n_1 inserted into Eq. (81), we can write $f_1(v)$ as

$$f_1 = \frac{ieE}{m}\left[\frac{f_o'(v)}{\omega + i\nu - kv} - \frac{i\nu}{kv_{th}^2} Z'(\zeta_o)\frac{f_o(v)}{\omega + i\nu - kv}\right] \quad . \tag{91}$$

The parallel electron current

$$j_z = -e\int_{-\infty}^{\infty} v f_1(v) dv \tag{92}$$

for a Maxwellian distribution is then

$$j_z = \frac{n_o e^2}{m}\frac{iE}{kv_{th}}\frac{1}{\sqrt{\pi}}\left[\int_{-\infty}^{\infty}\frac{d}{du}(e^{-u^2})\frac{udu}{u-\zeta} - \frac{i\nu}{kv_{th}} Z'(\zeta_o)\int_{-\infty}^{\infty}\frac{u}{u-\zeta}e^{-u^2}du\right] \quad . \tag{93}$$

This can be written in terms of the integrals I_1 and I_2, as defined below:

$$j_z = \frac{i\epsilon_o\omega_p^2 E}{kv_{th}}\left(I_1 - \frac{i\nu}{kv_{th}} Z'(\zeta_o) I_2\right) \quad . \tag{94}$$

Integration by parts yields I_1 and I_2 in terms of $Z(\zeta)$:

$$\begin{aligned} I_1 &= \frac{1}{\sqrt{\pi}}\int_{-\infty}^{\infty}\frac{u}{u-\zeta}\frac{d}{du}(e^{-u^2})du = -\frac{1}{\sqrt{\pi}}\int_{-\infty}^{\infty} e^{-u^2}\frac{d}{du}\left(\frac{u}{u-\zeta}\right)du \\ &= -\frac{1}{\sqrt{\pi}}\int_{-\infty}^{\infty} e^{-u^2}\frac{-\zeta}{(u-\zeta)^2}du = \zeta Z'(\zeta) \end{aligned} \tag{95}$$

$$I_2 = \frac{1}{\sqrt{\pi}}\int_{-\infty}^{\infty}\frac{ue^{-u^2}du}{u-\zeta} = -\frac{1}{2\sqrt{\pi}}\int_{-\infty}^{\infty}\frac{e^{-u^2}}{(u-\zeta)^2}du = -\frac{1}{2}Z'(\zeta) \quad . \tag{96}$$

Eq. (94) then becomes

$$\begin{aligned} j_z &= \frac{i\epsilon_o\omega_p^2 E}{kv_{th}}\left[\zeta Z'(\zeta) + \frac{i\nu}{2kv_{th}} Z'(\zeta_o)Z'(\zeta)\right] \\ &= \frac{i\epsilon_o\omega_p^2 E}{\omega}\zeta_o Z'(\zeta)\left[\zeta + \frac{i}{2}\frac{\nu}{\omega}\zeta_o Z'(\zeta_o)\right] \quad . \end{aligned} \tag{97}$$

To obtain a tractable expression for j_z, we write ζ as

$$\zeta = \frac{\omega + i\nu}{kv_{th}} = \zeta_o\left(1 + \frac{i\nu}{\omega}\right) \tag{98}$$

and expand $Z'(\zeta)$ about ζ_o:

$$Z'(\zeta) = Z'(\zeta_o) + (\zeta - \zeta_o)Z''(\zeta_o) = Z'(\zeta_o) + \frac{i\nu}{kv_{\rm th}}Z''(\zeta_o) \quad . \tag{99}$$

Thus, for $\zeta - \zeta_o \ll 1$, we have

$$j_z = \frac{i\epsilon\omega_p^2 E_z}{\omega}\zeta_o^2 Z'(\zeta_o)\left[1 + \frac{i\nu}{kv_{\rm th}}\frac{Z''}{Z'}\right]\left[1 + \frac{i\nu}{\omega} + \frac{i}{2}\frac{\nu}{\omega}Z'(\zeta_o)\right] \quad . \tag{100}$$

A further simplification results from assuming $\zeta \gg 1$, or $\omega/k \gg v_{\rm th}$. The asymptotic expansion of $Z'(\zeta)$ is

$$\zeta^2 Z'(\zeta) = 1 + \frac{3}{2}\frac{1}{\zeta^2} + \ldots - 2i\sqrt{\pi}\zeta^3 e^{-\zeta^2} \quad . \tag{101}$$

The $Z''(\zeta_o)$ term then

$$\frac{\nu}{kv_{\rm th}}\frac{Z''}{Z'} \simeq \frac{\nu}{kv_{\rm th}}\frac{-2}{\zeta_o^3}\zeta_o^2 = -\frac{2\nu}{\omega} \quad . \tag{102}$$

Evaluating j_z to first order in ν/ω, we obtain

$$\begin{aligned} j_z &= \frac{i\epsilon_o\omega_p^2 E_z}{\omega}\zeta_o^2 Z'(\zeta_o)\left(1 - \frac{i\nu}{\omega}\right) \\ &= \frac{i\epsilon_o\omega_p^2}{\omega}E_z\left(1 - \frac{i\nu}{\omega} - 2i\sqrt{\pi}\zeta^3 e^{-\zeta^2}\right) \quad . \end{aligned} \tag{103}$$

Comparing this with the fluid result from Eq. (62),

$$j_z = \frac{i\epsilon_o\omega_p^2}{\omega}E_z\left(1 - \frac{i\nu}{\omega}\right) \quad , \tag{104}$$

we see that the Landau term gives an effective rate equal to

$$\nu_{LD} = 2\sqrt{\pi}\omega\zeta^3 e^{-\zeta^2} \quad . \tag{105}$$

The total effective collision frequency is then

$$\nu_{eff} = \nu + \nu_{LD} \quad . \tag{106}$$

The corresponding effective resistivity is

$$\eta_{LD} = \frac{\nu_{LD}}{\epsilon_o\omega_p^2} = \frac{\omega}{\epsilon_o\omega_p^2}2\sqrt{\pi}\zeta^3 e^{-\zeta^2} \quad , \tag{107}$$

and the damping length for Landau damping is

$$L_{LD} = \frac{\omega_c}{\nu_{LD} T} = \omega_c / 2\sqrt{\pi}\omega T \zeta^3 e^{-\zeta^2} \quad . \tag{108}$$

One would expect that Landau damping would dominate over collisional damping if $\nu_{LD} > \nu$. Though the exact expression for ν_{LD} in terms of $Z'(\zeta)$ would continue to increase as ζ is decreased, the asymptotic approximation, Eq. (105), reaches a maximum at $\zeta = (3/2)^{\frac{1}{2}}$, or $\zeta^3 \exp(-\zeta^2) = 0.41$. Since the waves effectively do not propagate for smaller ζ, this value can be used to estimate the effectiveness of Landau damping when ω/k is adjusted to match the thermal velocity of the main electron distribution. Thus

$$\nu_{LD}(\max) \simeq 2\sqrt{\pi}(0.41)\omega = 1.45\omega \quad . \tag{109}$$

The electron-ion collision frequency is approximately

$$\nu_{ei} = 2.9 \times 10^{-12} n_o Z \ln\Lambda / T_e^{3/2} \sec^{-1} \quad . \tag{110}$$

where T_e is in eV and n_o in m^{-3}. Taking $Z = 1$, $T_e = 3$, and $\ln\Lambda = 10$, we find that the breakeven density at which $\nu = \nu_{LD}(\max)$ is

$$n_c = 2.6 \times 10^{11}\omega = 1.63 \times 10^{12} f \quad . \tag{111}$$

Thus, Landau damping should be the dominant dissipation mechanism for densities below about $5 \times 10^{19}\ m^{-3}$ for $f \simeq 30$ MHz.

C. Energy deposition

Finally, we show that the energy dissipation is connected with the z component of $\mathbf{E}$ and is not necessarily peaked on axis. The energy loss per unit volume is $\mathbf{j} \cdot \mathbf{E}$, but the transverse components of $\mathbf{j}$ amd $\mathbf{E}$ will not contribute to this, because $\mathbf{j}$ is parallel to $\mathbf{B}$ [Eq. (12)] while $\mathbf{E}$ is perpendicular to $\mathbf{B}_\perp$ [Eq. (31)], and hence $\mathbf{j}_\perp \cdot \mathbf{E}_\perp = 0$. The loss rate is then

$$-\frac{dW}{dt} = \langle \mathbf{j} \cdot \mathbf{E} \rangle = \langle j_z E_z \rangle \quad . \tag{112}$$

From Eqs. (2) and (66) we see that $\mathbf{j} = (\beta_1/\mu_o)\mathbf{B}$, where β_1 is given by Eq. (70). To lowest order in the damping, we may take $\beta_1 = \alpha$ here. Eqs. (44) and (105) then give

$$Re(j_z) = (2\alpha/\mu_o) T A J_m(Tr) \sin\psi \tag{113}$$

$$Re(E_z) = -(2\alpha/\mu_o) T A \frac{\omega}{\epsilon_o \omega_p^2} \left(\cos\psi - \frac{\nu}{\omega} \sin\psi \right) J_m(Tr) \quad , \tag{114}$$

where ψ is the phase $(m\theta + kz - \omega t)$. Thus

$$\langle j_z E_z \rangle = \frac{2A^2\nu}{\epsilon_o \omega_p^2} \left[\frac{\alpha}{\mu_o} T J_m(Tr) \right]^2 \quad . \tag{115}$$

According to this formula, the $m = 0$ mode deposits its energy mainly at $r = 0$, while the $m = 1$ mode heats the plasma preferentially at $r/a = 0.48$, where $J_m(Tr)$ has its maximum. In the Landau damping regime, edge heating is even more pronounced because of the density dependence of ν_{LD}/ω_p^2. In practice, the $m = 1$ mode is usually found to heat the plasma mostly at the center. Considerations of discharge physics — diffusion, temperature profile, and burnout of neutrals — would probably explain the discrepancy.

As a check on self-consistency, we can show that term in Eq. (115) is primarily responsible for the damping rate of the wave. The wave energy density is

$$W = \langle B^2/2\mu_o \rangle + \langle \epsilon_o E^2/2 \rangle + K.E. \quad . \tag{116}$$

The kinetic energy (K.E.) of the particles is negligible because the ions do not move and the electrons have only a slow $\mathbf{E} \times \mathbf{B}$ drift. Eq. (31) shows that the electric field energy, even including the electrostatic part, is smaller than the magnetic energy by $(\omega/kc)^2$ and can be neglected. From Eqs. (44) to (46) one can see that the magnetic energy, integrated over radius, is dominated by B_z; thus we have

$$\langle B^2 \rangle \simeq \langle B_z^2 \rangle = 2A^2 T^2 J_m^2 \quad , \tag{117}$$

$$W \simeq A^2 T^2 J_m^2 / \mu_o \quad . \tag{118}$$

The energy W changes at the rate $2Im(\omega) = -2v_g Im(k)$, where ν_g is the group velocity. The dispersion relation Eq. (9) shows that v_g is equal to ω/k except for the weak dependence of α on k. Thus we have approximately

$$\frac{dW}{dt} = 2Im(\omega)W = -2v_g Im(k)W \simeq -2(\omega/k)Im(k)W \quad , \tag{119}$$

$$-\frac{dW}{dt} = 2\frac{\omega}{k}\frac{\nu T}{\omega_o}\frac{A^2T^2}{\mu_o}J_m^2 = \frac{2A^2\nu}{\epsilon_o\omega_p^2}\alpha T \left[\frac{T}{\mu_o} J_m(Tr) \right]^2 \quad , \tag{120}$$

where we have used Eqs. (9) and (78) for ω/k and $Im(\omega)$. We see that Eqs. (115) and (120) are identical for $\alpha \simeq T$.

V. DESIGN OF PLASMA SOURCES

For design purposes, it is sufficient to neglect k^2 relative to T^2 in Eq. (14) and let $\alpha \simeq T$. The dispresion relation Eq. (9) then becomes

$$\frac{\omega}{k} = \frac{TB_o}{\mu_o e n_o} \tag{121}$$

where T is given by the approximate boundary condition $J_1(Ta) \simeq 0$ [Eqs. (36) and (37)] for the $m = 0, 1$ modes to be

$$T = 3.83/a \quad . \tag{122}$$

The first step is to choose the tube radius a and the phase velocity ω/k. If ω/k is chosen to be near $v_{\rm th}$, the wave will be strongly damped by Landau damping. On the other hand, the presumed advantage of helicon sources is the direct acceleration of primary electrons by wave-particle interactions. In that case, one would choose ω/k to be near the velocity of the ionizing electrons. Let E_f be the electron energy (in eV) to which the wave is to be matched. Then we have

$$\frac{\omega}{k} = \left(\frac{2eE_f}{m}\right)^{\frac{1}{2}} = 5.93 \times 10^5 E_f^{\frac{1}{2}} \ \ m/sec. \tag{123}$$

Using Eqs. (122) and (123) in Eq. (121) and converting to useful units, we obtain the B/n value

$$\frac{B_G}{n_{13}} = 31.2 E_f^{\frac{1}{2}} a_{cm} \ , \tag{124}$$

where B_G is in gauss, n_{13} in units of 10^{13} cm^{-3}, and a_{cm} in cm. For the most common case of discharges in argon, which has a peak in the ionization cross section at $E_f = 50$ eV, one would have

$$B_G/n_{13} = 220 a_{cm} \ , \qquad \omega/k = f\lambda = 4.19 \times 10^6 \ \ m/sec. \tag{125}$$

We see that B/n depends only on tube radius. For instance, a 10-cm diameter helicon source producing 10^{13} cm^{-3} densities would require a field of about 1kG. The density that is achievable depends on the rf power available to overcome the losses; these, in turn, depend on the neutral density, the tube radius, and the magnetic field (Chen, 1989).

The choice of frequency or wavelength is more flexible. The frequency is usually taken to be the industrial frequency of 13.56 MHz or one of its harmonics or subharmonics, and the one to choose depends on the aspect ratio of the antenna. An antenna which has both $k_\parallel$ and $k_\perp$, such as the Nagoya Type III antenna (Watari et al. 1978) has a coupling coefficient which increases as $k_\perp^2/k_\parallel^2$ (Chen, 1981); that is, as $(T/k)^2$. Let us define the aspect ratio, or gain factor, G to be

$$G \equiv \frac{T}{k} = \frac{3.83}{a}\frac{\lambda}{2\pi} = 0.61\frac{\lambda}{a} \quad . \tag{126}$$

A reasonable value to start with is $G = 8$, which gives a gain of 64. Eq. (126) then gives $\lambda = 13.1a$, and Eq. (125) gives, for argon, $f = 32/a_{cm}$ MHz. Table 1 shows the standard frequency that would be used for each range of tube diameter. Note that the plasma may choose its own diameter if the frequency is too high for the tube diameter used. This may be the reason that experiments often show (Sec. VI) a discharge that is concentrated along the axis, using less than the diameter available.

Once the frequency has been chosen, the other parameters can be calculated exactly. Eq. (123) gives

$$\lambda = 5.93 \times 10^5 E_f^{\frac{1}{2}}/f \quad m \quad , \tag{127}$$

and Eq. (126) gives the resulting antenna aspect ratio G. When G is not large, a more accurate value of T can be obtained for the $m = 1$ mode by iterating Eq. (35) or using Eq. (40). This value of T can then be used in Eq. (14) to obtain a better value for α, and thus, from Eq. (9), an accurate value for B/n. Fig. 4 shows such results for the $m = 0$ and 1 modes for various tube diameters as a function of phase velocity in units of $\sqrt{E_f}$, where $E_f = \frac{1}{2}m(\omega/k)^2$. Also shown in Fig. 4 is the total damping length $L_d = (1/L_c + 1/L_{LD})^{-1}$, calculated from Eqs. (79) and (108). In the region of large E_f, L_c dominates and is proportional to $\sqrt{E_f}$, as predicted by Eq. (79). For small $\sqrt{E_f}$, Landau damping dominates and is essentially exponential in $\sqrt{E_f}$. Note, however, that L_d has been calculated for the thermal electrons, not the primaries; and it is not necessary to make L_d comparable to the length of the discharge. In the original version of this paper (Chen, 1985), we surmised that the jumps in density seen experimentally were caused by the sudden increase in thermal Landau absorption when T_e and k jumped to large values that made ω/kv_{th} small. Subsequent data show that this is probably not the case. The values of B/n reported in the next section suggest that E_f lies in the range where L_d is much longer than the discharge, so that the wave is damped mainly by the acceleration of fast electrons. The computed value of L_d, therefore, need not be considered seriously in the design of helicon sources.

VI. RELATION TO EXPERIMENT

We have shown that helicon modes in a bounded, uniform plasma can have parallel phase velocities matched to the velocities of either thermal or hyperthermal electrons. We conjecture that the observed efficiency of helicon plasma generators is caused by the direct

acceleration of "primary" electrons to ionizing energies. Before applying our results to experiment, however, we should be aware that the present analysis is incomplete and may be insufficiently accurate in several respects.

1. Electron inertia. The effect of electron inertia is given by the factor γ defined in Eq. (68). Perpendicular inertia gives the electron gyromotion and leads to another root of the dispersion relation, $\beta_2 \simeq 1/2\gamma$ [Eq. (67)], which is essentially a cyclotron wave in a cylinder (Trivelpiece-Gould mode). Parallel inertia gives rise to an E_z even in the absence of dissipation [the first term of Eq. (114)]; but this term is out of phase with j_z and therefore does not contribute to damping. Its main effect is to shift the frequency by an amount $\alpha\gamma$ [Eq. (69], which is of order $(T/k)(\omega/\omega_c)$. These effects have been pointed out by Davies (1970) and reconsidered recently by Chen (1989b).

2. Polarization. Whistler waves in free space can only be right-hand polarized, but low-frequency whistlers in a cylinder (helicons) can also be left-hand polarized. Our analysis applies equally well to positive and negative values of m. Since $J_{-m} = \pm J_m$, the boundary condition of Eq. (35) is the same for $m < 0$ except for a change of sign in the small correction term in $J'_m(Ta)$, which is of order T/k. Indeed, one can construct modes which are nearly linearly polarized. This point will be amplified in a separate paper. As the frequency is lowered toward the ion gyrofrequency, however, the left-hand component will be much more affected by ion motions than the right-hand component, which rotates in the direction opposite to ion gyrations.

3. Ion motions. The assumption of infinite ion mass will break down as ω is lowered toward the lower hybrid frequency ω_{lh}. However, ω_{lh} is a resonant frequency of the plasma only for waves with $k_{||}/k_{\perp}$ smaller than $(m/M)^{\frac{1}{2}}$, so ion motions should not greatly alter the helicon dispersion relation at that frequency. As the frequency approaches the ion gyrofrequency Ω_c, left-hand polarized helicon waves would turn into ion cyclotron waves; but we would expect right-hand polarized helicons to be relatively unaffected, with a frequency change typically less than a factor of 2.

4. Non-uniform plasma. When the equilibrium density or magnetic field varies with radius, the parameter α is a function of r, and Eq. (11) has to be solved numerically. If the plasma is also inhomogeneous in the z direction, Eq. (11) is a differential equation in two dimensions. In what follows, we assume that B_o is uniform and that the average density $\langle n_o(r) \rangle$ can be used for n_o.

5. Energy transfer to primaries. The calculated Landau damping length [Eq. (108)] is rather long in most experiments. The rf energy is coupled directly to the primary electrons, but the trapping and acceleration of the primaries in the wave and the scattering and finite

gyroradius effects on them require a kinetic treatment which is beyond the scope of this paper.

6. Discharge physics. The plasma which is created by an rf antenna depends not only on the dispersion relation of the waves but also on diffusion and mobility, ionization by a distribution of fast electrons, collisional and Landau damping, antenna coupling, and so forth. In particular, the behavior of the ionizing electrons — the effects listed in the previous paragraph — are difficult to predict and are best studied experimentally.

The most extensive studies of helicon sources have been conducted by Boswell and his collaborators. It was recognized early on (Boswell, 1970) that $m = 1$ antennas could produce large peak densities $\hat{n}$ of order 4×10^{12} cm^{-3} with only 600W of 8-MHz power. However, the system was clearly not optimized, since inserting $a = 5$cm, $B = 750$G and $\langle n \rangle = 2 \times 10^{12}$ cm^{-3} into Eq. (124) leads to $E_f = 578$eV, which is well beyond the ionization maximum. In a later experiment with the same diameter, Boswell *et al.* achieved nearly $\hat{n} = 10^{14}$ cm^{-3}. The most complete measurements reported by Boswell (1984) were in argon, with $a = 5$cm, $L = 120$cm, $f = 8.6$MHz, $B \leq 1.6$kG, and an $m = 1$ antenna of half-wavelength 25cm. Thus the antenna is optimized to excite waves corresponding to $E_f = 53$eV. Indeed, the plasma was observed to be essentially 100% ionized on axis. The reported values of $\langle n \rangle$, however, were too low for agreement with Eq. (124). At 750G and $\langle n \rangle = 1.2 \times 10^{12}$cm^{-3}, for instance, E_f would be 1.6 keV. The computed value of E_f is so sensitive to n, however, that using the peak density of 5×10^{12}cm^{-3} would lead to the reasonable value $E_f = 92$ eV. The efficiency of absorption of the rf energy was 1000 times what would be expected from collisions. Landau damping can explain the efficiency if the density was underestimated. In this experiment the wave pattern was observed in both the radial and axial directions. As B was increased, n followed a constant B/n curve, but not continuously. The density jumped from one value to the next; perhaps this is connected with standing wave patterns in the axial or radial directions.

Evidence for the ionization mechanism described in this paper may have been seen unintentionally in an ion cyclotron heating experiment in the RFCXX magnetic mirror device in Nagoya, Japan [Sato *et al.* (1983), Okamura *et al.* (1986)]. By using two Nagoya Type III antennas 90° apart, it was possible to excite either left-hand polarized ($m = -1$) or right-hand polarized ($m = +1$) modes in the uniform 10-kG field of the central cell. Other parameters were $a = 5$ cm, $P_{rf} = 400$kW, $f = 13.7$MHz, and hydrogen gas. As was intended, ion cyclotron heating was observed with $m = -1$ over a narrow range of magnetic field, with $0.9 < \omega/\Omega_c < 1$. The tube was filled uniformly with plasma at $T_e \simeq 20$eV and $n \simeq 2 \times 10^{12}$ cm^{-3}. With $m = +1$, the polarization which rotates against the ion gyration direction, it was found surprisingly that the density was much higher, peaking on axis at

7×10^{13} cm^{-3} in a narrow column of radius 1.5 cm. The ions were not heated, and T_e was also lower at $\simeq$ 10eV. Efficient ionization was observed over a much wider range of magnetic field ($0.55 < \omega/\Omega_c < 1$), and the density scaled linearly with the gas puffing rate. Since the right-hand mode is insensitive to ion cyclotron effects, all these observations are consistent with helicon ionization with the $m = +1$ mode. If we take $\langle n \rangle = 3 \times 10^{12}$ cm^{-3}, $B = 10^4$G, and $a = 5$ cm, Eq. (124) predicts $E_f = 458$eV, which is rather large. However, it is reasonable to assume that the ion mass effects slow down the wave by a factor of order 2; in this case E_f becomes $\simeq$ 100eV, which is close to the ionization maximum for hydrogen. The only observation which does not fit this picture is that the energy deposition is peaked on axis.

After the first version of this paper was circulated (Chen, 1985), three groups have investigated the Landau damping of helicon waves. Shoji (1986,1987,1988) achieved $\hat{n} > 10^{13}$ cm^{-3} in argon, with $a = 5$ cm, $P_{rf} = 1$KW, $f = 8 - 10$ MHz, and $B = 0.5 - 2$ kG. As in most other experiments, only a low-density, non-resonantly produced plasma was produced at low rf power ($P_{rf} < 300$W); but the density jumped discontinuously with increasing P_{rf}, as would be expected when n/B reaches a value fitting the helicon dispersion relation. Shoji also tested helical antennas with various numbers of turns but found no advantage over the straight, $\frac{1}{2}$-wavelength Nagoya Type III variety. An unexpected dependence on ion mass was found in Shoji's experiments. Efficient ionization characteristic of helicon sources was found only with A and Xe. With lighter gases — Ne, He, D_2, and H_2 — ionization was strong only in a narrow peak near the lower hybrid frequency.

Evidence for the production of fast electrons was seen by Chen and Decker (1989c, 1990) in an experiment with $a = 1$cm, $B = 0 - 1000$G, $f = 31$ MHz, and argon gas. Peak densities of order 3×10^{12} cm^{-3} were measured with 800W of rf power. A floating endplate was found to be charged to $V_f \simeq -250$V though T_e was only a few eV, and $|V_f|$ *increased* as the endplate was moved *away* from the antenna, suggestive of wave acceleration. The measured value of B/n was consistent with $E_f = 50$eV. Furthermore, as B was lowered, $|V_f|$ took a sudden jump downwards at $B = 40$G, exactly the field at which a 50-eV electron would have a Larmor radius equal to the tube radius. Apparently, the primary electrons acquire perpendicular velocity by elastic scattering, and a portion of them is lost when magnetic confinement is lost.

In recent work geared to industrial applications, Perry and Boswell (1989) made a plasma suitable for plasma etching, obtaining an SF_6 plasma of density $> 10^{12}$ cm^{-3} with $a = 7.5$ cm, $B = 50$G, $f = 13.56$ MHz, and $P_{rf} = 1$kW. If we assume $\langle n \rangle = 3 \times 10^{11}$ cm^{-3}, Eq. (124) yields $E_f = 50.7$ eV, a very reasonable value. Zhu and Boswell (1989) excited an argon laser in a 4.5-cm diam by 160 cm long tube, achieving $n = 8 \times 10^{13}$ cm^{-3} at $P_{rf} = 3.5$kW, $B = 900$G, and $f = 7$ MHz. The density profile showed a HWHM of only 0.6 cm, and it is

possible to choose different values of a and of $\langle n \rangle$ to use in Eq. (124). The resulting values of E_f range from 14 to 100 eV, a range consistent with the observed excitation of Ar^{+} and Ar^{++} lines.

These recent experiments have given preliminary confirmation of the Landau acceleration mechanism in helicon wave plasma generators, indicating that the efficient production of a controllable fast electron population may be possible for industrial applications.

This work was supported by the National Science Foundation, Grants ECS 87-12089 and 89-01249.

REFERENCES

Boswell, R.W. (1970) *Phys. Lett.* **33A**, 457.

Boswell, R.W., Porteus, R.K., Prytz, A., Bouchoule, A., and Ranson, P. (1982) *Phys. Lett.* **91A**, 163.

Boswell, R.W. (1984) *Plasma Phys. and Controlled Fusion* **26**, 1147.

Boswell, R.W. and Henry, D. (1985) *Appl. Phys. Lett.* **47**, 1095.

Boswell, R.W. and Porteus, R.K. (1987a) *Appl. Phys. Lett.* **50**, 1130.

Boswell, R.W. and Porteus, R.K. (1987b) *J. Appl. Phys.* **62**, 3123.

Bowers, R., Legendy, C., and Rose. F.E. (1961) *Phys. Rev. Lett.* **7**, 339.

Chen, F.F. (1981) TRW Report Task II-3552 (unpublished).

Chen, F.F. (1985) Australian National Univ. Report ANU-PRL IR 85/12, *unpublished.*

Chen, F.F. (1987) in *Proceedings of the 1987 Int'l Conf. on Plasma Physics, Kiev, USSR,* ed. by A.G. Sitenko (World Scientific, Singapore), Vol. A, p. 797.

Chen, F.F. (1989a) *Lasers and Particle Beams* **7**, 551.

Chen, F.F. (1989b) UCLA Report PPG-1270 *(unpublished).*

Chen, F.F. and C.D. Decker (1989c) *Bull. Amer. Phys. Soc.* **34**, 2128.

Chen, F.F. and C.D. Decker (1990) in *Proceedings of the 1989 Int'l Conf. on Plasma Physics,* New Delhi, India, to be published.

Davies, B.J. (1970) *Plasma Phys.* **4**, 43.

Davies, B.J. and Christiansen, P.J. (1969) *Plasma Phys.* **11**, 987.

Harding, G.N. and Thonemann, P.C. (1965) *Proc. Phys. Soc.* **85**, 317.

Klozenberg, J.P., McNamara, B., and Thonemann, P.C. (1965) *J. Fluid Mech.* **21**, 545.

Lehane, J.A. and Thonemann, P.C. (1965) *Proc. Phys. Soc.*, **85**, 301.

Okamura, S. et al. (1986) *Nuclear Fusion* **26**, 1491.

Perry, A.J. and Boswell, R.W. (1989) *Appl. Phys. Lett.* **55**, 148.

Rose, F.E. Taylor, M.T. and Bowers, R. (1962) *Phys. Rev.* **127**, 1122.

Sato, T. *et al.* (1983) Nagoya Univ. Inst. of Plasma Physics Report IPPJ-653.

Shoji, T. (1986) IPPJ Annual Review, Nagoya University, Japan, 67.

Shoji, T. (1987) IPPJ Annual Review, Nagoya University, Japan, 63.

Shoji, T. (1988) IPPJ Annual Review, Nagoya University, Japan, 83.

Watari, T. et al. (1978) *Phys. Fluids* **21**. 2076.

Woods, L.C. (1962) *J. Fluid Mech.* **13**, 570.

Woods, L.C. (1964) *J. Fluid Mech.* **18**, 401.

Zhu, P., and Boswell, R.W. (1989) *Phys. Rev. Lett.* **63**, 2805.

TABLE 1

approx. diam.	freq.
1.5 cm	40.68 MHz
2	27.12
4	13.56
10	6.78
20	3.39

Initial choice of operating frequency as a function of tube diameter (for argon)

FIGURE CAPTIONS

1. Electric field line patterns for the $m = 0$ mode. (a) 3-D representation; (b) cross sections at $(k/\alpha)ctn(kz - \omega t) = 1/3$ (left) and 1 (right).

2. Electric field line patterns for the $m = 1$ mode. (a) 3-D representation; (b) detailed pattern for $k/\alpha = 1/3$. Line spacing is indicative of field strength only at $y = 0$.

3. For the $m = 1$ mode, variation with k/α of (A) $T/3.83$, (B) r_o, and (C) r_m.

4. Dispersion curves for helicon waves for four combinations of frequency f and tube radius a. In each case, curve (a) is B_o/n_o for the $m = 1$ mode vs. $E_f^{\frac{1}{2}}$, where B_o is in gauss, n_o in units of 10^{11} cm^{-3}, and E_f is $\frac{1}{2}m(\omega/k)^2$ in eV. Curve (b) is the same for the $m = 0$ mode. Curve (c) is the damping length L_d vs. $E_f^{\frac{1}{2}}$ for $T_e = 3$eV, but the scale factor and the assumed density are different for each case. Curve (d) is a cross-plot of E_f as a function of Bn; $E_f/10$ in eV is given by the abscissa. Case 1: $f = 27.12$ MHz, $a = 1$ cm, $n_o = 5 \times 10^{12}$cm^{-3}, and (c) is $L_d/10$ in cm. Case 2: $f = 13.56$ MHz, $a = 2$ cm, $n_o = 5 \times 10^{13}$ cm^{-3}, and (c) is $L_d/20$ in cm. Case 3: $f = 6.78$ MHz, $a = 5$ cm, $n_o = 10^{14}$ cm^{-3}, and (c) is $L_d/200$ in cm. Case 4: $f = 3.39$ MHz, $a = 10$ cm, $n_o = 10^{13}$ cm^{-3}, and (c) is $L_d/100$ in cm.

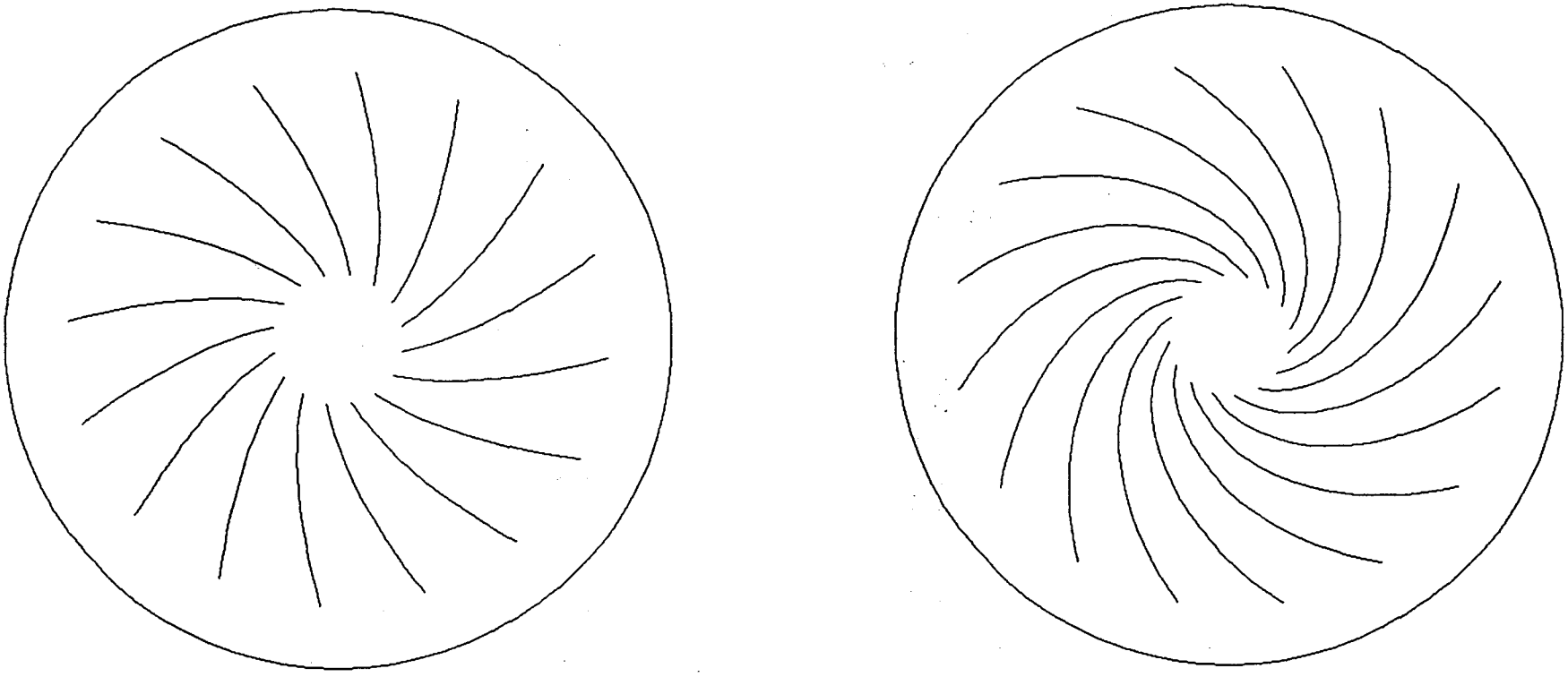

Fig. 1b

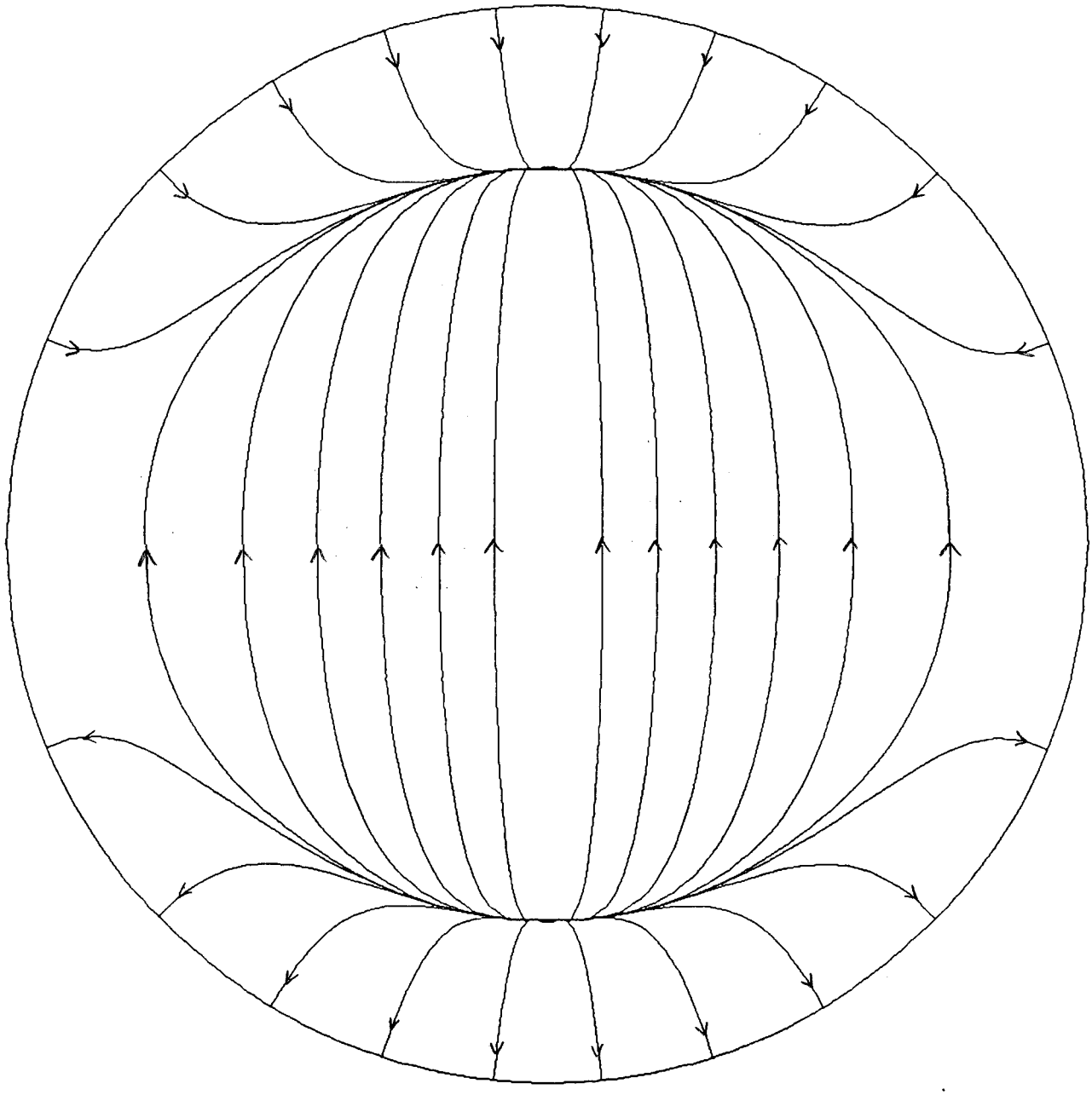

Fig. 2b

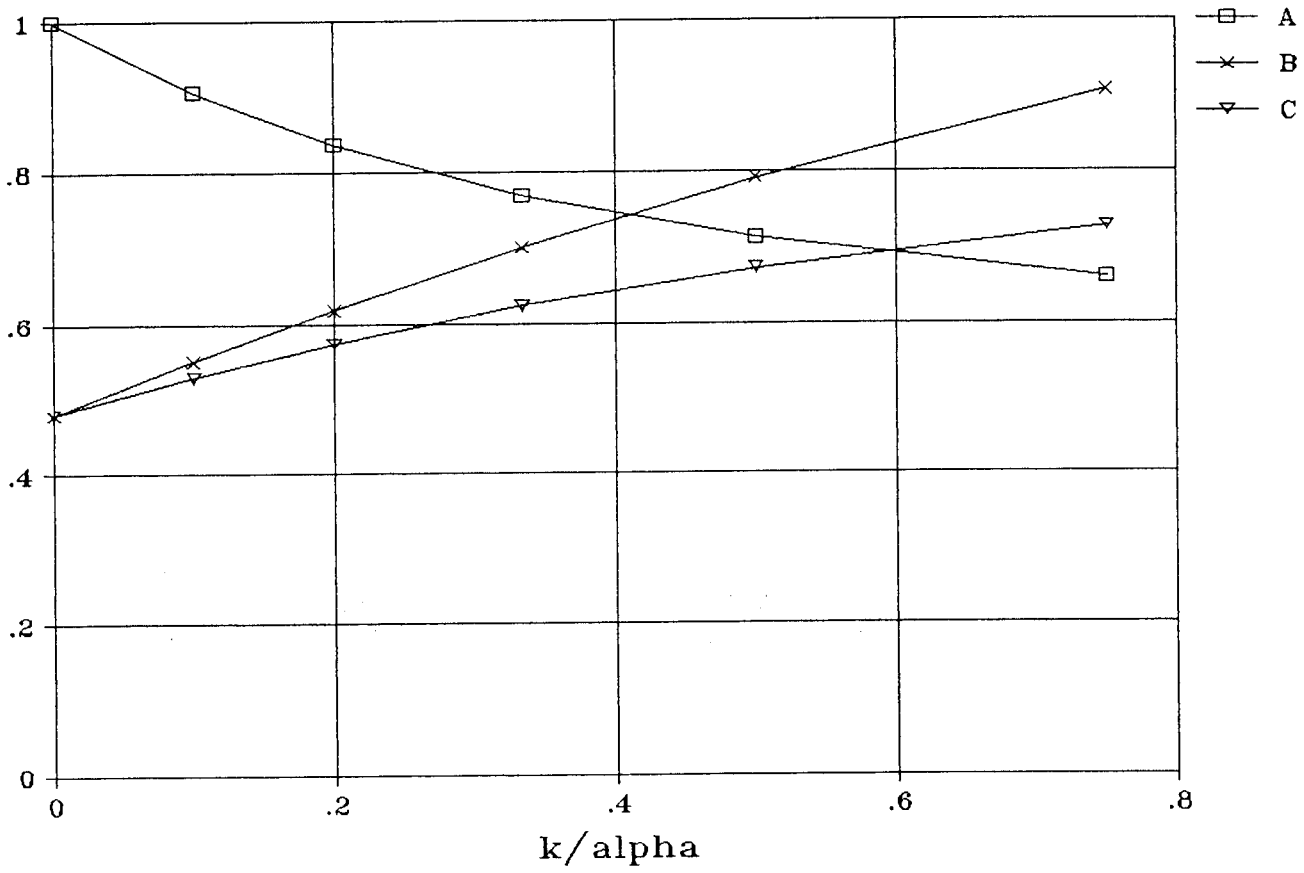

Fig. 3

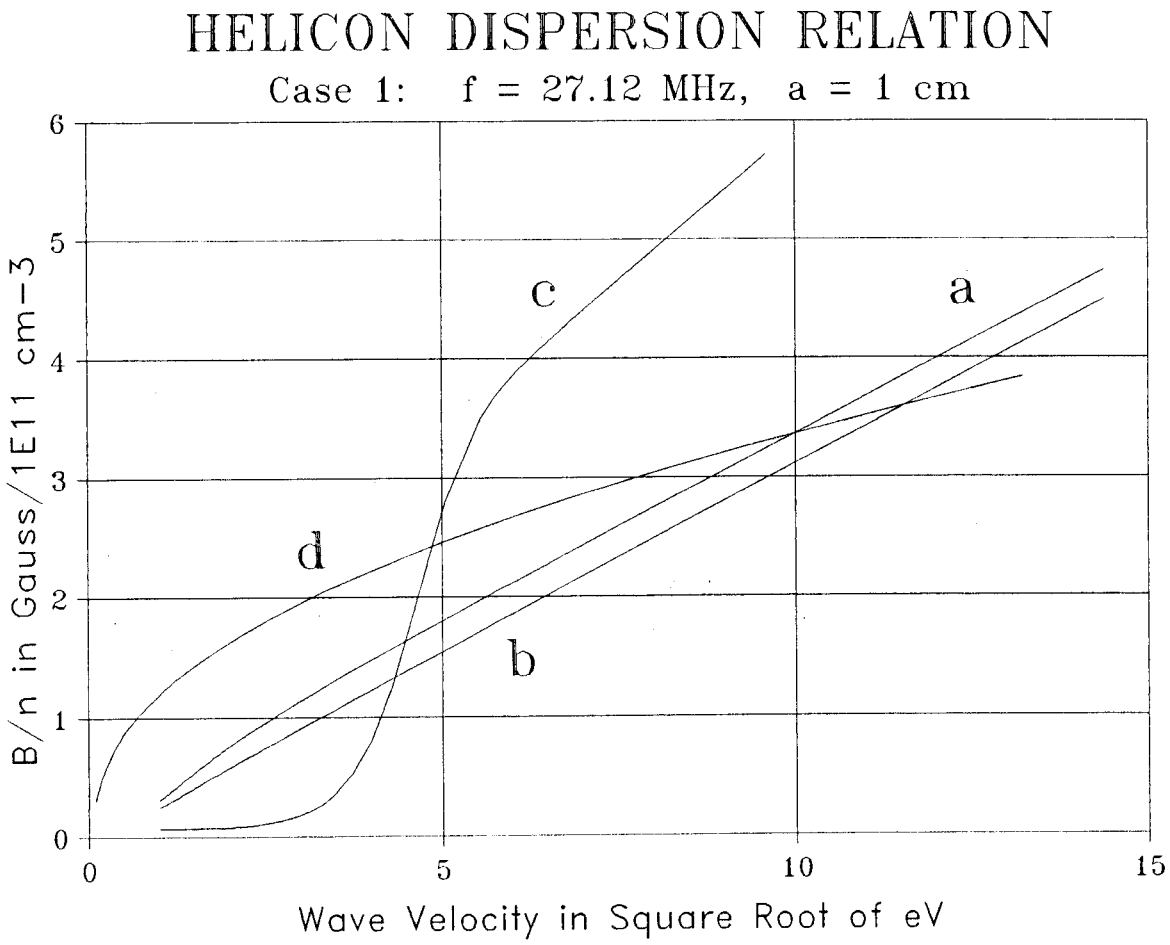
HELICON DISPERSION RELATION
Case 1: f = 27.12 MHz, a = 1 cm
B/n in Gauss/1E11 cm-3
Wave Velocity in Square Root of eV
0
1
2
3
4
5
6
0
5
10
15
a
b
c
d

Fig. 4a

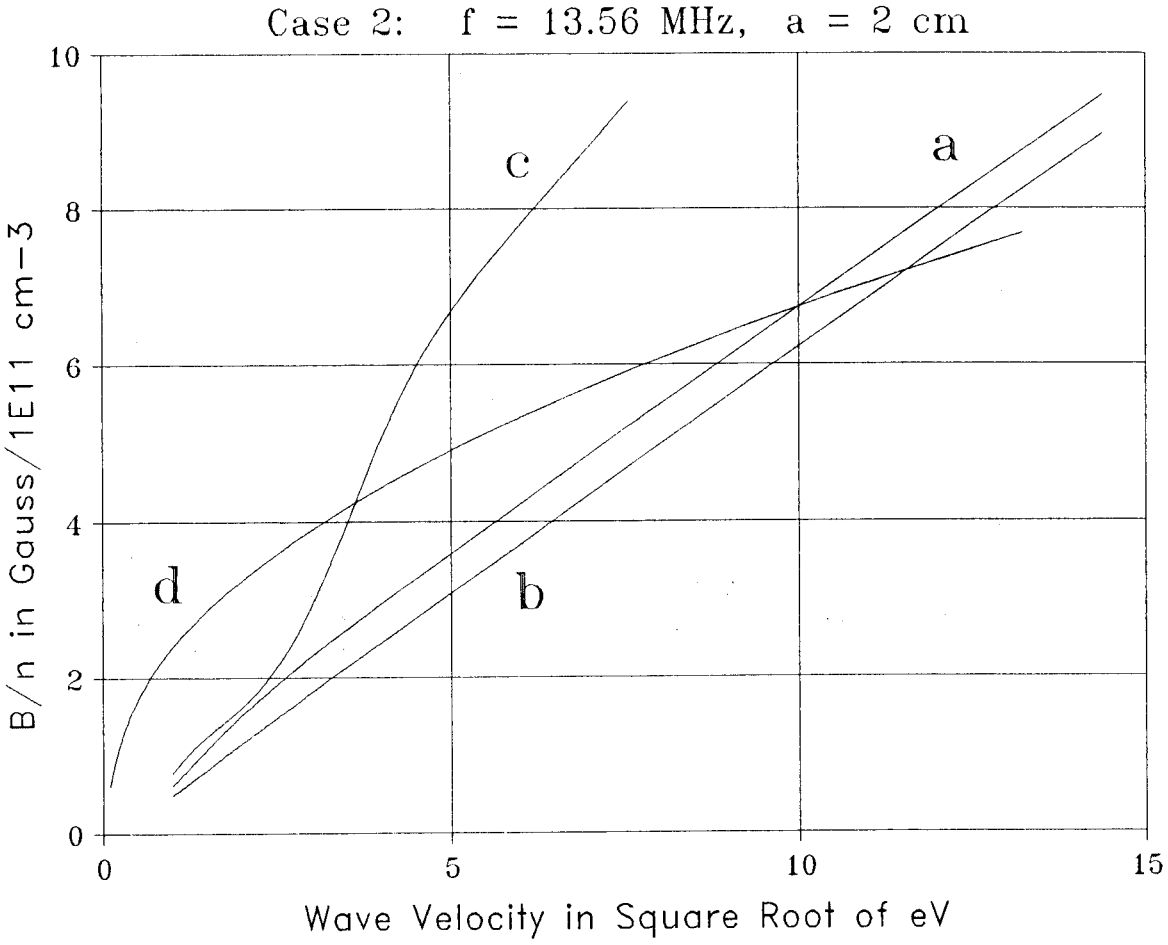
Case 2: f = 13.56 MHz, a = 2 cm
B/n in Gauss/1E11 cm-3
Wave Velocity in Square Root of eV
0
2
4
6
8
10
0
5
10
15
a
b
c
d

Fig. 4b

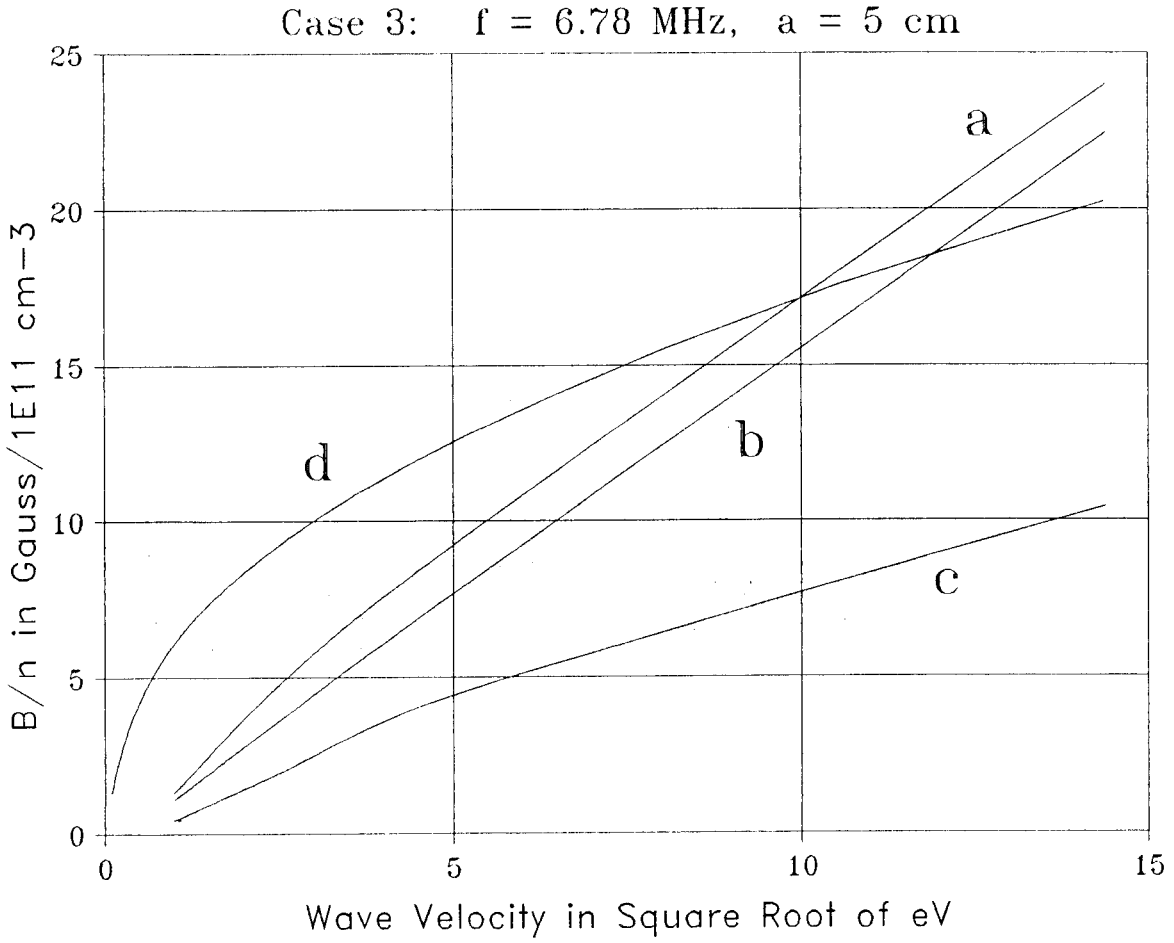
Case 3: f = 6.78 MHz, a = 5 cm
B/n in Gauss/1E11 cm-3
Wave Velocity in Square Root of eV
0
5
10
15
20
25
a
b
c
d

Fig. 4c

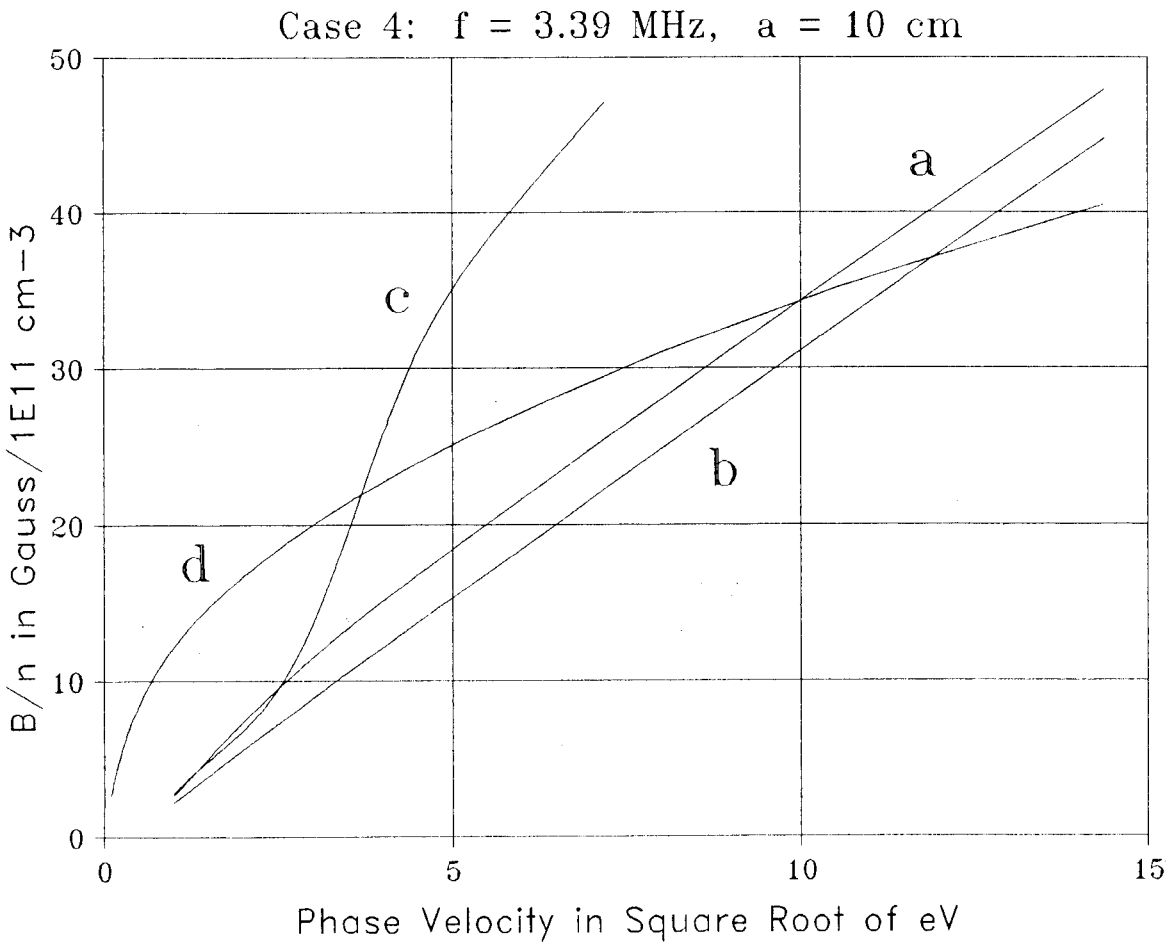
Case 4: f = 3.39 MHz, a = 10 cm
B/n in Gauss/1E11 cm-3
Phase Velocity in Square Root of eV
0
10
20
30
40
50
0
5
10
15
a
b
c
d

Fig. 4d